HAL
open science

Modeling of entorhinal cortex and simulation of epileptic activity: insights into the role of inhibition-related parameters.

Etienne Labyt, Paul Frogerais, Laura Uva, Jean-Jacques Bellanger, Fabrice Wendling

To cite this version:

Etienne Labyt, Paul Frogerais, Laura Uva, Jean-Jacques Bellanger, Fabrice Wendling. Modeling of entorhinal cortex and simulation of epileptic activity: insights into the role of inhibition-related parameters.. IEEE Transactions on Information Technology in Biomedicine, 2007, 11 (4), pp.450-61. inserm-00183634

HAL Id: inserm-00183634

https://inserm.hal.science/inserm-00183634

Submitted on 30 Oct 2007

HAL is a multi-disciplinary open access archive for the deposit and dissemination of scientific research documents, whether they are published or not. The documents may come from teaching and research institutions in France or abroad, or from public or private research centers.

L'archive ouverte pluridisciplinaire **HAL**, est destinée au dépôt et à la diffusion de documents scientifiques de niveau recherche, publiés ou non, émanant des établissements d'enseignement et de recherche français ou étrangers, des laboratoires publics ou privés.

HAL author manuscript
IEEE Transactions on Information Technology in Biomedicine 2007;11(4):450-61

Published in IEEE Transactions on Information Technology in Biomedicine
2007; 11(4):450-61
Special issue on Biomedical Informatics

HAL author manuscript inserm-00183634, version 1

Modeling of entorhinal cortex and simulation of epileptic activity: insights into the role of inhibition related parameters

E Labyt, P Frogerais, L Uva[+], JJ Bellanger, F Wendling

Laboratoire Traitement du Signal et de L'Image, Inserm U642, Rennes University 1, 35042 Rennes, France

[+] : Department Experimental Neurophysiology, Istituto Nazionale Neurologico, via Celoria 11, 20133 Milan, Italy

Key words: Computational model, neuronal population, parameter identification, epilepsy, entorhinal cortex, experimental model

Corresponding author:

Doctor Fabrice Wendling
Laboratoire de Traitement du Signal et de l'Image (LTSI)
INSERM U642 - Campus Beaulieu
Université de Rennes 1
35042 Rennes cedex
phone: +33 3 23 23 65 30; fax: +33 3 23 23 69 17
e-mail: fabrice.wendling@univ-rennes1.fr

**This material is presented to ensure timely dissemination of scholarly and technical work.
Copyright and all rights therein are retained by authors or by other copyright holders.
All persons copying this information are expected to adhere to the terms and constraints invoked by each author's copyright.
In most cases, these works may not be reposted without the explicit permission of the copyright holder.**

HAL author manuscript inserm-00183634, version 1

Abstract

This paper describes a macroscopic neurophysiologically-relevant model of the entorhinal cortex (EC), a brain structure largely involved in human mesio-temporal lobe epilepsy. This model is intervalidated in the experimental framework of ictogenesis animal model (isolated guinea-pig brain perfused with bicuculline). Using sensitivity and stability analysis, an investigation of model parameters related to GABA neurotransmission (recognized to be involved in epileptic activity generation) was performed. Based on spectral and statistical features, simulated signals generated from the model for multiple GABAergic inhibition related parameter values were classified into eight classes of activity. Simulated activities showed striking agreement (in terms of realism) with typical epileptic activities identified in field potential recordings performed in the experimental model. From this combined computational/experimental approach, hypotheses are suggested about the role of the different types of GABAergic neurotransmission in the generation of epileptic activities in EC.

HAL author manuscript inserm-00183634, version 1

I. Introduction

In mesio-temporal lobe epilepsy (MTLE), a subtype of temporal lobe epilepsy (TLE) [1], stereo-electroencephalographic (SEEG, intracerebral depth electrodes) recordings in intractable patients showed that seizures may originate from the entorhinal cortex (EC) [2]. More recently, this brain structure has been shown to play an important role in the interictal/ictal transition in MTLE [1, 3].

Several evidences arguing that EC is largely involved in MTLE have also been obtained from field potential recordings in experimental animal models [4-7]. These animal models are particularly adapted to investigate the role of the EC in epileptic activity generation because this structure belongs to the "paleocortex", a well conserved part of the cortex during the species evolution. So, it can be assumed that the intrinsic organization of EC is very similar between animal species and humans and consequently, studies from epilepsy acquired animal models can be very informative about human epilepsy pathophysiology.

SEEG signals and field potentials can be considered as macroscopic recordings. Both reflect overall dynamics rising from interconnected populations of principal neurons and interneurons. Actually, an important issue consists in relating these macroscopic recordings to circuit and synaptic transmission mechanisms (type of post-synaptic receptors involved, kinetics of postsynaptic responses, efficacy of synaptic transmission) underlying epileptic activities. This issue can be addressed using a computational modeling approach based on cytoarchitectonic and neurobiological knowledge about the anatomical structure under analysis. In the present study, we describe a realistic model of the EC which offers the possibility to investigate the simulated field potential activity as a function of the temporal dynamics of its postsynaptic components. Bifurcation and stability analysis of the model are then used to generate hypotheses about synaptic mechanisms involved in the transition from normal to epileptic activity in an in vivo model (guinea-pig isolated brain preparation).

HAL author manuscript inserm-00183634, version 1

II. Background and objectives

The purpose of this study is to interpret epileptic activities (interictal and ictal) recorded from the EC in an animal model: the isolated guinea-pig brain perfused with bicuculline [8, 9] through realistic modeling of field potential activity. The model is based on EC cytoarchitectonic and neurobiological data reported in literature and summarized in appendix. In this work, we focused on the analysis of GABAergic synaptic interactions between principal cells and interneurons populations included in the model. Indeed, an important role in generation of epileptic activities (interictal and ictal) has recently been attributed to GABA-mediated neurotransmission. This hypothesis is issued from several studies investigating epileptic activities recorded from hippocampus in experimental models [10-12] and in epileptic patients [11, 13, 14]. Additional evidences have also been obtained from different modeling approaches validated with combined real recordings. Using the modeling (at cellular level) of a neuronal network, Traub et al showed that GABAa receptor-mediated inhibition was crucial for shaping gamma oscillations [15]. In another study [16], a physiologically-relevant macroscopic model of hippocampus permitted to reveal that fast onset ictal activity was explained by the impairment of dendritic $GABA_a$ receptor-mediated inhibition with slow kinetics. Based on experimental animal recordings, a role of GABAergic inputs from interneurons has also been suggested in production of epileptic activities within the EC [5, 17, 18].

Consequently, we specifically studied GABAergic synaptic interaction related parameters in the model. We performed both sensitivity and stability analysis in order to identify model parameter evolutions which explain observed transitions of dynamics in real signals (for example, from interictal spikes to fast activity at seizure onset and from fast onset to ictal burst activity).

HAL author manuscript inserm-00183634, version 1

III. Computational model

A. *Level of modeling*

A macroscopic modeling approach (neuronal population level) was chosen because this level allows simulation of signals that can be directly compared to real signals (field potentials reflect overall dynamics rising from interconnected populations of principal neurons and interneurons). Theoretical description of the approach is described in [19] and its first use for electrophysiological data interpretation were reported by Freeman [20] and Lopes Da Silva [21, 22]. More recently, this class of models was exploited in various neurophysiological or clinical studies [23, 24] [16, 25] [26] .

This macroscopic approach differs from Traub's [15] which uses a large number (up to more than one thousand) of neurons and interneurons (each one represented by a complex multi compartmental model) for each subpopulation. Indeed, in macroscopic models, populations of cells composed by different subpopulations (typically principal cells and interneurons) which interact via synaptic connections are considered. In other words, each subpopulation may be seen as a unique 'lumped-parameter neuron model' while a population model is obtained from interconnection of these neuron models. The complexity of the corresponding mathematical model is hence dramatically decreased.

Each lumped-parameter model includes inputs (either inhibitory or excitatory) interpreted as average firing rates of action potentials (averaged on both time and space). Inputs are simply defined by a lowpass linear filters whose output represent the average postsynaptic potential and whose time constant can be specifically adapted to the kinetics of receptors present in the postsynaptic membrane. The output of the model is interpreted as a mean frequency of action potentials fired at the soma. It is obtained from the weighted summation of postsynaptic potentials fed into a static nonlinear operator which accounts for threshold and saturation effects.

B. *Entorhinal cortex computational model*

Based on available data about the cellular and network organization of the EC (see appendix, figure 1 and table 1), we introduced i) *NP* specific subpopulations of neurons (pyramidal cells, stellate cells) and interneurons which are encountered in deep and superficial layers of this brain structure and ii) a set of intra-layer and inter-layer interaction links between these *NP* subpopulations (Figure 1 A).

Regarding synaptic interactions in this network, we distinguished excitatory postsynaptic activities (glutamatergic) from inhibitory postsynaptic activities (GABAergic or glycinergic). GABAergic transmission is itself mediated by GABAa (with slow and fast kinetics) and GABAb receptors.

In the model, the dynamics of the set of the *NP* interconnected subpopulations correspond to the state trajectory of a system of *NP* interconnected differential equation subsystems (one subsystem per subpopulation). Each subsystem equation corresponds to a multiple input/one output system (as represented in figure 1 B for subpopulation number *p*) and that can be described by equation (1). For the subpopulations influenced by noise, the term n_p in (1) is a random input (positive mean gaussian white noise) which models non specific afferences on principal cells only (i.e. pyramidal - P_1, P_2 - and stellate - *St* – subpopulations). Otherwise, if no 'external noise' acts on the subpopulation, a zero value must be substituted for variable n_p in (1) :

$$\frac{d}{dt}\underline{y}_p(t) = f_p^{\theta_p}[\underline{y}_p(t), \{o_k(t), k \in I_p\}, n_p(t)],\ \underline{y}(t) \in R^{2+2|I_p|}, t \in R^+, p = 1..NP \quad (1)$$

$$f_p^{\theta_p} : R^{2+2|I_p|+|I_p|+1} \rightarrow R^{2+2|I_p|} \quad (2)$$

HAL author manuscript inserm-00183634, version 1

where p denotes the considered subpopulation index, $\underline{y}_p$ denotes the state vector of this subpopulation, $\{o_k(t), k \in I_p\}$ is the list of outputs from afferent subpopulations and $|I_p|$ (cardinal of I_p) is the number of afferent subpopulations.

As illustrated in figure 1-B, for given subpopulation number p, the relationship between presynaptic afferent input(s) ($\{o_k\}$ and n_p or $\{o_k\}$ only) and population firing output (o_p) can be defined as in equation (3) and (4):

$$o_p(t) = S^{\mu_p}(x_p(t)) \quad (3)$$

$$x_p(t) = \sum_{k \in I_p} C_k^p.(o_k * h_k^p)(t) + (n_p * h_{n_p}^p)(t) \quad (4)$$

where C_k^p accounts for the average number of synaptic contacts from population k to population p, $x_p(t)$ represents the input potential at the soma which is a summation (symbol * denotes the convolution product) of linearly filtered versions of afferent inputs $o_k(t)$ and of the input noise n_p (if present). Filters are themselves defined by their respective impulse responses detailed in equations (5) and (6):

$$h_k^p(t) = M_k^p \frac{t}{\tau_k^p} \exp(-t/\tau_k^p) \text{ if } t \geq 0, = 0 \text{ otherwise }, k \in I_p \quad (5)$$

$$h_{n_p}^p(t) = M_{n_p}^p \frac{t}{\tau_{n_p}^p} \exp(-t/\tau_{n_p}^p) \text{ if } t \geq 0, = 0 \text{ otherwise }. \quad (6)$$

where M_k^p is a positive (excitatory input) or negative (inhibitory input) constant equal to the product of maximal value of $h_k^p(t)$ and of the neperian logarithm basis e (the larger M_k^p, the more efficient the synaptic link $k \to p$) and τ_k^p is a time constant (the larger τ_k^p, the smoother the input) which accounts for the rise and decay time of postsynaptic potentials, in accordance with receptor kinetics and propagation delays along dendritic trees.

HAL author manuscript inserm-00183634, version 1

The function S^{μ_p} defined by equation (7) and which appear in the right part of figure 1 B,

$$S^{\mu_p}(x) = \frac{2e_0^p}{1+\exp(r^p(v_0^p - x))} \in \left]0, e_0^p\right[,\ x \in R,\ \mu_p = (r^p, e_0^p, v_0^p) \quad (7)$$

is a sigmoid function (nonlinear positive increasing function) which models nonlinear threshold (minimum pre-somatic mean potential level for action potential firing) and saturation (maximal firing rate) effects as constants $2e_0^p$, v_0^p and r^p respectively define the maximum firing rate, the post-synaptic potential corresponding to a firing rate equal to e_0^p and r^p the steepness of the sigmoid.

The link between convolution kernels h_k^p or $h_{n_p}^p$ in (5) and (6) and differential equation systems (1) is given by the equivalence between on one hand $z_{k,1}^p(t) = (h_k^p * o_k)(t)$ and $z_{n,1}^p(t) = (h_{n_p}^p * n_p)(t)$ and on other hand the order two differential equation systems:

$$\{\ \frac{d}{dt} z_{k,1}^p(t) = z_{k,2}^p(t)\ \ ,\ \frac{d}{dt} z_{k,2}^p(t) = -\frac{2}{\tau_k^p} z_{k,2}^p(t) - \frac{1}{(\tau_k^p)^2} z_{k,1}^p(t) + \frac{M_k^p}{\tau_k^p} o_k(t)\ \ \} \quad (8)$$

$$\{\frac{d}{dt} z_{n,1}^p(t) = z_{n,2}^p(t)\ \ ,\ \frac{d}{dt} z_n^p(t) = -\frac{2}{\tau_{n_p}^p} z_n^p(t) - \frac{1}{(\tau_{n_p}^p)^2} z_n^p(t) + \frac{M_{n_p}^p}{\tau_{n_p}^p} n_p(t))\ \} \quad (9)$$

where the pair of 'local' states variables $\{ z_{k,1}^p(t)\ \ , z_{k,2}^p(t) = \frac{d}{dt} z_{k,1}^p(t)\ \ \}, k \in I_p$ and $\{ z_{n,1}^p(t), z_{n,2}^p(t) = \frac{d}{dt} z_{n,1}^p(t) \}$ (if noise present) are introduced and pooled to form the subpopulation state vector $\underline{y}_p$:

$$\underline{y}_p^T = [z_{1,1}^p, z_{2,1}^p, .., z_{1,|I_p|}^p, z_{2,|I_p|}^p, 0, 0] \quad (10)$$

$$\underline{y}_p^T = [z_{1,1}^p, z_{2,1}^p, .., z_{1,|I_p|}^p, z_{2,|I_p|}^p, z_{n,1}^p, z_{n,2}^p] \quad (11)$$

Here, the last two components $z_{n,1}^p, z_{n,2}^p$ in (11) denote the two state variables associated with the convolution kernel $h_{n_p}^p$, similarly as in (8) but with n_p in place of o_k. These 2 components are taken into account only if input noise is present, i.e. only for index p

HAL author manuscript inserm-00183634, version 1

corresponding to subpopulations P1 , P2 and St. Otherwise, they are set to zero as in equation (10).

The conjoint activity of all subpopulations is represented by the time evolution of the global state vector $\underline{y} = [\underline{y}_1^T, .., \underline{y}_{NP}^T]^T$ in $R^{\dim(\underline{y})}$ with $\dim(\underline{y}) = \sum_{p=1..N_p} \dim(\underline{y}^p)$.

Parameters set θ^p in $f_p^{\theta_p}$ is $\theta^p = \{\mu_p, ((M_k^p, C_k^p, \tau_k^p), k \in I_p)\} \cup \{M_{n_p}^p, \tau_{n_p}^p\}$ (if noise present) or $\theta^p = \{\mu_p, ((M_k^p, C_k^p, \tau_k^p), k \in I_p)\}$ (if noise not present)

Finally the overall system of equations may be written as:

$$\frac{d}{dt}\underline{y}(t) = f^{\theta}[\underline{y}(t), \underline{n}(t)], \underline{y}(t) \in R^{\dim(\underline{y})}, t \in R^+, \ \underline{y}(0) = \underline{y}_0 \qquad (12)$$

where $\underline{y}_0$ denotes the initial state vector value and where the global vector parameter θ is the concatenation of the θ^p, $p = 1, .., N_p$.

C. *Stochastic nature of the model*

In this time-continuous model (12), the input vector $\underline{n}(t)$ is a positive mean Gaussian noise vector that pools the noise inputs $n_p(t)$ and that models non specific afferences from surrounding neuronal groups whose individual influences are not 'organized', i.e. not synchronous. Consequently, the model is governed by a set of stochastic nonlinear ordinary differential equations. However, if $\underline{n}(t)$ is substituted by the statistical mean of the input M_n in (3), we obtain a deterministic system of nonlinear ordinary differential equations:

$$\frac{d}{dt}\underline{y}(t) = f^{\theta}[\underline{y}(t), M_n], \ \underline{y}(t) \in R^{\dim(\underline{y})}, \ t \in R^+, \quad \underline{y}(0) = \underline{y}_0 \qquad (13)$$

which can be studied for stability (see results section).

D. Model output

In order to explore real data recorded with a field electrode, we must establish a correspondence between the electrode signals, say $X(t)$, and vector $\underline{y}(t)$ in (13). The

HAL author manuscript inserm-00183634, version 1

classical approach is to use the approximation $X(t) \approx h^T \tilde{y}(t), h \in R^{\dim(\underline{y})}$ where the non null components of column parameter vector h are such that $h^T \underline{y}(t)$ is equal to a weighted sum of functions $x_p(t)$ (postsynaptic potentials) in which index p corresponds to pyramidal cell subpopulations [27]. This choice is relevant because spatial alignment of pyramidal neurons ('in palissades') implies that vector summation of dendritic current dipoles corresponds to the summation of their modules in this case.

E. Model parameters

As mentioned in section II (Background and objectives), we only focus on GABAergic interactions. Consequently, variations of maximal postsynaptic potential parameters M_k^p will be considered only when index k corresponds to GABAergic neurotransmission (I_1, I_2 or I_3). Standard values of I_1, I_2, I_3, I_4. glycine mediated neurotransmission) and E (glutamate mediated neurotransmission) as well as corresponding time constants τ_k^p are given in table 2. For each subpopulation with non specific afferences, $\tau_{n_p}^p$ will be set to τ_e value given in table 2.

Furthermore, for two connections $(k \to p)$ and $(k' \to p')$ on target subpopulations p and p', we impose $M_k^p = M_{k'}^{p'}$ if k and k' correspond to the same type of neurotransmission.

The other parameters in θ remain fixed. Regarding connectivity parameters C_k^p, values are given in table 3. The value of $\mu_p = (r^p, e_0^p, v_0^p)$ is independent of p and is equal to (0.56 mV^{-1}, 2.5 s^{-1}, 6 mV). Finally in the sequel we will denote $\theta_0 = (I_1, I_2, I_3)$ the triplet of free parameters.

HAL author manuscript inserm-00183634, version 1

IV. Model parameter identification

Model parameter identification (or parameter estimation) is a difficult problem. It can be approached by elaborating a mapping procedure T which associates an observed sampled signal $X(t), t \in \{0, \Delta, .., (N-1)\Delta\} = \underline{X}$ an estimated value $\hat{\theta}_0 = T(\underline{X})$ for unknown parameter θ_0 with an estimation error criterion (like a mean square error, for example) that is expected as low as possible.

In order to build T, we introduced a K-dimensional feature vector $\underline{X} \to \hat{F} = G(\underline{X}) \in R^K$ and we defined T by minimization of a square error norm: $\hat{\theta}_0 = T(\underline{X}) = \arg\min_{\theta_0} \left\| \hat{F} - F(\theta_0) \right\|^2$ where $F(\theta_0) = E^{\theta_0}(\hat{F})$ (θ_0-dependant mathematical expectation of $\hat{F}$, so $\hat{F}$ is an unbiased estimator for F). The interesting aspect of this method is that the choice for $\hat{F}$ is open. The drawback is that computation of $F(\theta)$ calculus is generally intractable.

To overcome this difficulty, a possibility is to evaluate $\theta \to F(\theta)$ by means of simulated observations $\underline{X}_S^{\theta}(\underline{n})$ (where index S refers to 'Simulation' and where $\underline{n}$ is the random input noise vector in the model). For sufficient signal duration (number of samples) the evaluation $G(\underline{X}_S^{\theta}(\underline{n}))$ can then be put in place of $F(\theta)$ in $\left\| \hat{F} - F(\theta) \right\|^2$ to search $\hat{\theta}$ optimal value by mean of an optimization algorithm, under the assumptions that $\hat{F}$ is informative about the true value θ^* of θ (i.e. $\hat{F}$ must not be too different from $G(\theta)$) and that $\left| \frac{\partial}{\partial \theta} G(\theta^*) \right|$ is sufficiently large.

A. Activity maps

Assuming the two above conditions, we used a feature vector $\hat{F}$ and the error function $\left\| \hat{F} - G(\underline{X}_S^{\theta_0}(\underline{n}) \right\|^2$ to uncover, from simulations, disjoint regions in the space of free

HAL author manuscript inserm-00183634, version 1

parameters ($\theta_0 \in R^3$), each region being associated to a particular type of model activity. Then, activities reflected in real signals as well as transitions between activities are interpreted as possible paths connecting corresponding regions in the space of free parameters. As this space is of dimension 3, paths are displayed on the (I_1, I_2) plane, for different values of I_3. In the results section, (I_1, I_2) planes are referred to as 'activity maps'.

B. Classification procedure

Activity maps are obtained from a supervised classification procedure. This procedure starts from a partitioning of the domain of possible values of θ_0 in N_C classes $\{C_1,..,C_{NC}\}$ defined from the similarity between simulated and real activity (one class per activity). This partitioning provides a set $\{\tilde{F}_1,..,\tilde{F}_{NC}\}$ $(\tilde{F}_i \in R^3)$ of reference values in the feature space. Then, for a large set $(\theta_{0k}, \underline{n}_k), k=1,\ldots,N$ (N depending on the discretization of θ_0) such that $\theta_{0k}, k=1,\ldots,N$ constitutes a 'sufficiently dense' exploration of the θ_0 space and where $\underline{n}_k, k=1,\ldots,N$ are independent realizations of the input noise in the model, the procedure affects θ_{0k} to class C_j if and only if the square distance $d^2(\tilde{F}_i, G(\underline{X}_S^{\theta_{0k}}(\underline{n}_k)))^2 = \left\|\tilde{F}_i - G(\underline{X}_S^{\theta_{0k}}(\underline{n}_k))\right\|^2, i=1,..,NC$, is minimum for $j=i$.

This approach was motivated by two considerations: 1) in experiments, visual inspection of real signals reveals a limited number of types of activity and 2) in a large amount of simulations with different values of θ_k, simulated signals displayed only a small number (equal to 8) of types of dynamics.

C. Determination of reference centers $\{\tilde{F}_1,..,\tilde{F}_{NC}\}$

NC reference values $\theta_{01}^*,..,\theta_{0NC}^*$ for which characteristic dynamics are obtained, when X(t) is simulated, are first retained. Let $\{\underline{X}_S^{\theta_{0r}}(n_r), r \in J_k\}, k=1,..,N_C$ be N_C sets of independently simulated signals (eq. 4) where, for each k, $\theta_{0r}, r \in J_k$ are randomly selected in a sphere of

HAL author manuscript inserm-00183634, version 1

radius R centered on θ_{0k}^{*}. Then, for each class C_k, feature reference $\tilde{F}_k$ is chosen to be equal to the arithmetic mean of the $T(\underline{X}_S^{\theta_{0r}}(\underline{n}_r)), r \in J_k$.

D. Definition of feature vector $\hat{F} = (\hat{F}_1, \hat{F}_2, \hat{F}_3, \hat{F}_4, \hat{F}_5, \hat{F}_6)^T$

Both morphological and spectral signal characteristics were used in the definition of feature vector $\hat{F}$. The former are essentially based on the amplitude distribution of signals which was assumed to be discriminant as it varies from one type of activity to another (figure 2, last column). The first three features were obtained from partitioning of the amplitudes of signals normalized by the maximum of their modulus. Number of bins and thresholds were optimized in terms of separation between different classes of activity. This procedure led to define three amplitude intervals, [-0.6, -0.05], [-0.05, 0.05] and [0.05, 0.6]. Features $\hat{F}_1$, $\hat{F}_2$, and $\hat{F}_3$ correspond to the percentage of samples whose amplitude value are included in the above intervals, respectively.

Let $\underline{X} = X_0,...,X_{N-1}$ be N samples taken in the observed or simulated signal, and let $\underline{X}r = Xr_0,...,Xr_{N-1}$ be the "rescaled" signal where: $Xr_k = \dfrac{X_k}{\max\limits_{0 \le k \le N-1}(|X_k|)} \in (-1,1)$

We introduce $\hat{F}_1 = FR(\underline{X}r, -0.6, -0.05)$, $\hat{F}_2 = FR(\underline{X}r, -0.05, 0.05)$ and $\hat{F}_3 = FR(\underline{X}r, 0.05, 0.6)$

where $FR(\underline{Y}, \alpha, \beta) = \dfrac{1}{N} card\{Y_k / \alpha < Y_k \le \beta\}$, $0 < \alpha < \beta < 1$, for any real sequence $\underline{Y} = Y_0 ... Y_{N-1}$.

The last three features were defined to characterize the frequency content of signals and more particularly, their power into specific frequency sub-bands. As for amplitude features, tests were performed to determine the number of frequency sub-bands and boundaries. Best results were obtained for 3 sub-bands, [3, 12], [13, 17] and [18, 50] Hz. Features $\hat{F}_4$, $\hat{F}_5$, and $\hat{F}_6$

HAL author manuscript inserm-00183634, version 1

correspond to the signal power in the above intervals obtained from computation of the power spectral density (PSD, figure 2, middle column) using the averaged periodogram method.

Let us consider $\overline{PER}(\underline{X}, f), f \in \{0,1,...,255\}$ as the block averaged periodogram obtained with 256 points FFT and 50% overlap between adjacent blocks (which is an estimator of the PSD). We then define, for $0 \le f_1 < f_2 \le 127$, the normalized band power on $\{f_1,...,f_2\}$ as $NBP(f_1, f_2) = (\sum_{f_1 \le f \le f_2} \overline{PER}(X, f)) / (\sum_{0 \le f \le 127} \overline{PER}(X, f))$ and the last three features as $\hat{F}_4 = NBP(3,12)$, $\hat{F}_5 = NBP(13,17)$ and $\hat{F}_6 = NBP(18,50)$.

Finally the feature vector is defined as $\hat{F} = (\hat{F}_1, \hat{F}_2, \hat{F}_3, \hat{F}_4, \hat{F}_5, \hat{F}_6)^T$.

V. Experimental data

Experimental data were obtained from brains of Hartley guinea pigs (150-200g, Charles River, Calco, Italy) isolated and maintained *in vitro* by perfusion with a cold (4-10°C) oxygenated (95%) complex saline solution according to the standard procedure described elsewhere [28-30]. Experiments were performed at 32°C after gradually raising the temperature with 0.2°C/min steps. Extracellular recordings were performed in deep layers of the EC with 16-channels silicon probes (100 µm contact separation, provided by Jamille Hetcke, CNCT, University of Michigan, Ann Arbour, MI) inserted perpendicularly to EC lamination under direct visual control with a stereoscopic microscope. Focal epileptiform discharges in the limbic region were induced by 3-5 minutes arterial applications of the $GABA_a$ receptor antagonist, bicuculline (50 µM; SIGMA) diluted in the perfusion solution [9].

The viability of the isolated brains was tested by recording the responses evoked in the limbic cortices by stimulating the lateral olfactory tract [31-33]. At the end of the electrophysiological experiments, in order to verify the position of the electrodes, an

HAL author manuscript inserm-00183634, version 1

electrolytic lesion were made by passing a 30 µA current for 30 seconds between the two deepest contacts of the silicon probe. Further, this lesion was localized on 75-100µm thick coronal sections obtained from the isolated brain under exploration. The experimental protocol was reviewed and approved by the Committee on Animal Care and Use and by Ethics Committee of the Istituto Nazionale Neurologico.

From recordings performed in 10 isolated brains, eight classes of activities (numbered from 1 to 8) have been identified (Figure 3). Corresponding signals simulated by the model are displayed. It can be noticed that they closely resemble real field potentials. Class 1 refers to normal background activity as observed in real recordings before bicuculline perfusion. After injection of bicuculline, infrequent spikes (class 2) appear, and become rhythmic (class 3) before seizure begins. Class 4 corresponds to fast activity usually observed at the onset of seizure. Classes 5 and 6 respectively refer to frequent bursts (class 5) and infrequent (or sporadic) bursts activities which are classically observed during the seizure time-course. Finally, two other types of epileptic activities have been identified: spikes mixed to fast activity (class 7) which can be observed just before the seizure onset and polyspikes (class 8) encountered during ictal period.

VI. Results

Activity maps obtained for different values of I_3 ($GABA_b$ inhibition) are shown in figure 4. These activity maps represent the distribution of the eight classes of activity (detailed above) in the two-dimensional parameter plane I_1/I_2 ($GABA_{a\ slow}/GABA_{a\ fast}$ inhibitions). From visual inspection of these maps, we can notice that for high values of I_3, the model produces almost only background activity. Epileptic activities start to appear when I_3 decreases. All classes of epileptic activities are exclusively produced if I_3 is set below a threshold value (6.5 mV). Below this I_3 threshold value and considering low values of I_1, fast

HAL author manuscript inserm-00183634, version 1

onset activity, frequent and infrequent bursts are produced for high values of I_2 while the different spiking activities (spikes mixed to fast activity, polyspikes, spikes frequent and infrequent) are observed for low values of I_2. Beyond the I_3 threshold value, fast onset activity disappears while the amount of polyspikes activity increases. Finally, it can be noticed that the amount of frequent spikes as well as frequent burst activities decrease in favor of infrequent spikes and infrequent burst activities when I_3 rises. In other words, the frequency of spikes (for low values of I_2) and of burst (for high values of I_2) is controlled by the I_3 value in the model.

Activity maps can also be considered as a representation of bifurcations in the model, corresponding to transitions from one class of activity to another one. However, there are no bifurcations in the model for the transition from infrequent spikes or bursts to frequent spikes or bursts. Indeed, in these cases, the same activity is produced by the model and only the frequency of these activities is different.

We also performed a preliminary study of model stability (eq. 4) by analyzing noise independent properties. The model was recognized as experimentally stable if, for some random initial conditions, the state vector converged to a same fixed point in the absence of input noise fluctuations (standard deviation equal to zero). A more formal study of fixed points is beyond the scope of this paper. Results from stability study provided the limit values in the two-dimensional parameters plane I_1/I_2 separating the stable from the unstable parameter regions in the model. This limit (solid line) was superimposed on each activity map. As interestingly observed in figure 4, the unstable zone globally corresponds to values of I_1/I_2 parameters for which epileptic activities are produced by the model. The stable zone increases with parameter I_3 value.

HAL author manuscript inserm-00183634, version 1

The knowledge of activity maps generated from the model may be used to interpret temporal dynamics and transitions observed in real field potentials recorded from EC during the transition to seizure in the experimental animal model.

A first example corresponding to the seizure pattern which is encountered in most cases (named as typical) is given in figure 5. Eight steps (S_1- S_8) are distinguished according the pseudo-stationary nature of the activity reflected by the signal (Figure 5-A): normal background activity (S_1), infrequent spikes (S_2), more frequent spikes (S_3), rhythmic spikes (S_4), spikes mixed to fast activity (S_5), fast onset activity (S_6), frequent bursts (S_7) and finally, infrequent bursts (S_8). The observed transitions from background to infrequent spikes activity and then, between periods of epileptic activities can be represented on the activity maps as possible paths connecting corresponding regions of activity and which provide to a time-evolution for model parameters I_1, I_2 and I_3. All these paths are oriented from high to low values along the I_1 axis, denoting a reduction of $GABA_{a\ slow}$ inhibition and in a next step, from low to higher values along the I_2 axis and along the "virtual" I_3 axis, interpreted as an increase of $GABA_{a\ fast}$ and $GABA_b$ inhibitions.

In order to simulate time-series signals (figure 5-B) which temporal dynamics reproduce those observed in the real field potentials (figure 5-A), we chose one possible path drawn on activity maps shown in figure 5-C. Following this path, starting from standard I_1/I_2 values for which a background activity (step S_1) is simulated by the model, five successive decreases in I_1 value leads the model to generate realistic infrequent spikes (S_2) and then, frequency of spikes increases (S_3) until rhythmic spikes appears (S_4). Next, these rhythmic spikes mix to fast activity (S_5) until the emergence of fast activity (S_6) corresponding to the seizure onset. Afterwards, frequent burst activity is observed when I_2 and I_3 values increase (S_7). Finally, a

HAL author manuscript inserm-00183634, version 1

second increase in I_3 values leads to a slowing down of burst activity (S_8) before the seizure ends.

An interesting feature of the procedure is its capacity to also interpret another seizure pattern less frequently encountered in real recordings and characterized by a lack of rhythmic spikes and fast onset activity when seizure begins (figure 6-A). Using the same procedure, we defined two possible paths characterized by 6 steps (S_1-S_6) on the activity maps (Figure 6-C and 6-D). Starting from the same standard I_1/I_2 values (S_1) than in the precedent example, the first path (figure 6-C) leads to hypothesize that I_1 value ($GABA_{a\ slow}$ inhibition) decreases more abruptly and in a lesser extent (S_1 to S_4). So, three successive decreases in I_1 value result in the appearance of spikes (S_2) whose frequency increases (S_3) before the emergence of spikes mixed to fast activity (S_4). But the I_1 value does not sufficiently decrease such that fast activity at seizure onset is observed. Afterwards, as observed in the precedent seizure pattern, frequent burst activity (S_5) is generated when I_2 and I_3 values increase and finally, the burst activity slows down (S_6) consecutively to a further increase of parameter I_3 value. The second possible path (figure 6-D) leads to the hypothesis that the I_3 value ($GABA_b$ inhibition) might be higher in this experiment and remains constant. For this higher I_3 value, no fast onset activity is produced by the model. In this case, the three successive decreases in I_1 values (S_1 to S_4) lead the model to generate infrequent spikes (S_2), more frequent spikes (S_3) and then spikes mixed to fast activity (S_4). Appearance of the frequent burst activity is explained in the model by an increase in I_2 value and then, a re-increase in I_1 value results in the production of an infrequent burst activity before seizure termination. From these inhibition profiles, time-series signals shown in figure 6-B are produced by the model. As in the previous example, it can be noticed that this simulated signal is very realistic compared to the real field potential recording.

HAL author manuscript inserm-00183634, version 1

HAL author manuscript inserm-00183634, version 1

VII. Discussion and conclusion

In this study, we proposed a macroscopic computational model which produces vectorial signals corresponding to normal background activity and also to different types of epileptiform activities which are very realistic compared to real signals (extracellular field potentials) recorded from EC in the isolated guinea-pig brain during seizures induced by bicuculline perfusion. The macroscopic modeling level (based on a lumped parameter approach) chosen for this study seems us to be particularly suited to the nature of experimental recordings and human intracerebral recordings (i.e. SEEG). Indeed, the model output corresponds to a reflection of ensemble dynamics rising from macroscopic statistical interactions between interconnected neuronal sub-populations (pyramidal cells and interneurons) and therefore, it can be interpreted as extracellular field potentials recorded in animal models or in intractable patients under pre-surgery exploration.

A crucial step in the modeling is to determine parameters values and to validate modeling results. In this study, this step was achieved in interaction with real recordings from experimental guinea-pig model. Because it is very difficult to determine parameters values only from available experimental data, the parameters identification was addressed in this work using a systematic variation procedure of parameters values around standard values. This procedure was coupled to an automatic classification method of simulated signals based on their spectral and statistical features. Here, it needs to notice that this procedure has only been applied to model parameters related to the three types of GABAergic inhibition present in the model, based on convergent evidences that GABAergic synaptic interactions play a important role in generation of epileptic activities [5, 17, 18]. Amplitude of other average post-synaptic potentials (excitatory and Glycine-mediated inhibitory) as well as connectivity values were kept constant. In spite of these restrictions, our classification method resulted in very homogeneous classes of activities as it can be observed on activity maps. This last result

increases model's confidence as it suggests that there are not several possible parameters sets to generate one given type of activity identified from real recordings. Moreover, from these parameters sets, very realistic signals could be simulated. As exemplified with the two different seizure patterns, they provided a physiologically relevant interpretation of transitions between the different types of activity, either from the background activity to the period preceding the seizure onset (where spikes appears and increase in frequency) or during the seizure time-course itself. In terms of stability, this work also showed that instability in the model (globally corresponding to epileptic activities) was caused by introducing both a decrease of $GABA_{a\ slow}$ and $GABA_b$ receptor-mediated inhibitions. Beyond the validation of modeling results from real recordings, the model can also be used to generate testable hypothesis about possible mechanisms underlying the transition from background to epileptic activities. From this study, the role of $GABA_b$-mediated inhibition in the epileptic activities generation, in the decrease of burst frequency or in the process of seizure termination should be experimentally tested.

The model can also be considered as a valuable tool to advance in the understanding of pathophysiological mechanisms of human epilepsy. Indeed, the computational model integrates several types of knowledge: neurobiological (cellular organization, connections…), pharmacological (types of receptors, types of neurotransmitters, bicuculline effect) and physiological (role in generation of epileptic activities). As presented in this study, using modeling results, it has been possible to interpret field potentials in terms of synaptic interactions for different types of GABA receptors and therefore, to put forward hypothesis about the role of these types of GABA inhibitions in the generation of epileptic activities. For example, in the model, fast onset activity seems to be produced only if I_2 parameter value ($GABA_{a\ fast}$ receptor-mediated inhibition) is sufficiently high. The model acts as a bridge between the macroscopic observations (extracellular field potentials) and fine mechanisms at

HAL author manuscript inserm-00183634, version 1

synaptic level. Thus, this model could offer a good way to progress in the role of EC and mechanisms present within this brain structure involved in human MTLE. Another perspective is to use such models to represent the temporal dynamics of epileptic activity sources located in limbic structures. Indeed, electrical or magnetic potentials observed on electrodes positioned at the surface of the head can be computed, given some information about the spatial distribution of these sources and given a volume conductor model (forward problem). Such an approach could contribute to better interpretation of spatio-temporal dynamics reflected in MEG [34] or EEG [35] signals recorded in temporal lobe epilepsy.

Appendix: Cellular organization of entorhinal cortex

According with anatomo-functional description reported in previous works [36, 37], "superficial layers" (superficial to lamina dissecans (layer IV)) and "deep layers" (between lamina dissecans and the white matter) are represented in a superficial EC model and a deep EC model. The global EC model corresponds to superficial EC model interconnected to deep one (figure 1). In the sequel, we describe the cytology and network connectivity of the EC.

A. Principal excitatory neurons

Principal excitatory neurons in the entorhinal cortex consist in pyramidal cells localized in superficial layers (mainly in layer III) and deep layer (mainly layer V) and stellate cells localized in superficial layers (mainly layer II) [37-43]. Pyramidal neurons in deep layers project to pyramidal and stellate neurons in superficial layers [44], [45, 46]. In turn, they receive afferent inputs from pyramidal neurons in superficial layers [43].

B. Interneurons

The EC model includes two classes of interneurons: inhibitory and excitatory [47, 48]. Based on pharmacological studies, it has been shown that inhibitory interneurons project to four types of post-synaptic receptors: glycine receptors [49] [50]; $GABA_b$ receptors [51, 52];

HAL author manuscript inserm-00183634, version 1

and two kinetically distinct subtypes of $GABA_a$ receptors (fast and slow) [53] identified from recording of spontaneous inhibitory synaptic currents in EC interneurons (layers II and V). According with this assumption, spatially segregated synapses (axo-somatic and axo-dendritic) from inhibitory interneurons to pyramidal and stellate cells have been identified [43, 47, 54]. Taken together, these observations suggest that there are dendritic and somatic inhibition in the EC and according to previous works, dendritic inhibition would involve mainly $GABA_{a\ slow}$ receptors while somatic inhibition would involve mainly $GABA_{a\ fast}$ ones [55, 56].

All interneurons (inhibitory and excitatory) receive afferents excitatory inputs from stellate (only in superficial layers) and pyramidal cells [36, 53, 57]. An additional excitatory afferent input to GABAergic interneurons comes from excitatory interneurons [36, 53, 57]. In turn, excitatory interneurons receive inhibitory feedback from GABA interneurons via $GABA_a$ (slow and fast) receptors [36, 47, 48]. Moreover, glycinergic interneurons receive an inhibitory feedback from GABAergic interneurons via $GABA_{a\ slow}$ receptors [50].

C. Extra-entorhinal inputs

Pyramidal (in superficial and deep layers) and stellate cells receive an extrinsic excitatory input from subiculum, pre- and para-subiculum [58] as well as from CA1 [59-62], a subfield of hippocampus. Another extra-entorhinal input comes from neocortex and olfactory cortex [36] as well as subcortical structures [36, 63].

D. Entorhinal outputs

The main output pathway of EC originates from stellate cells and deep pyramidal neurons which give rise to the perforant route, projecting to dentate gyrus and CA3/CA2 hippocampal fields [43, 45, 46, 64]. The second EC output consists in the temporo-ammonic pathway from pyramidal neurons in superficial layers (mainly layer III) which send their axons predominantly to hippocampal field CA1 and the subiculum [36, 65, 66].

HAL author manuscript inserm-00183634, version 1

Acknowledgement

Experimental recordings were kindly provided by M de Curtis from the Istituto di Neurologica Carlo Besta – Milano. This study was funded by the French Foundation for Epilepsy Research (FFRE).

HAL author manuscript inserm-00183634, version 1

HAL author manuscript inserm-00183634, version 1

References

[1] F. Bartolomei, F. Wendling, J. Regis, M. Gavaret, M. Guye, and P. Chauvel, "Pre-ictal synchronicity in limbic networks of mesial temporal lobe epilepsy," *Epilepsy Res*, vol. 61, pp. 89-104, 2004.

[2] S. S. Spencer and D. D. Spencer, "Entorhinal-hippocampal interactions in medial temporal lobe epilepsy," *Epilepsia*, vol. 35, pp. 721-7, 1994.

[3] F. Bartolomei, M. Khalil, F. Wendling, A. Sontheimer, J. Regis, J. P. Ranjeva, M. Guye, and P. Chauvel, "Entorhinal cortex involvement in human mesial temporal lobe epilepsy: an electrophysiologic and volumetric study," *Epilepsia*, vol. 46, pp. 677-87, 2005.

[4] J. Bear and E. W. Lothman, "An in vitro study of focal epileptogenesis in combined hippocampal-parahippocampal slices," *Epilepsy Res*, vol. 14, pp. 183-93, 1993.

[5] M. Avoli, M. D'Antuono, J. Louvel, R. Kohling, G. Biagini, R. Pumain, G. D'Arcangelo, and V. Tancredi, "Network and pharmacological mechanisms leading to epileptiform synchronization in the limbic system in vitro," *Prog Neurobiol*, vol. 68, pp. 167-207, 2002.

[6] P. de Guzman, M. D'Antuono, and M. Avoli, "Initiation of electrographic seizures by neuronal networks in entorhinal and perirhinal cortices in vitro," *Neuroscience*, vol. 123, pp. 875-86, 2004.

[7] M. de Curtis and D. Pare, "The rhinal cortices: a wall of inhibition between the neocortex and the hippocampus," *Prog Neurobiol*, vol. 74, pp. 101-10, 2004.

[8] M. De Curtis, G. Biella, M. Forti, and F. Panzica, "Multifocal spontaneous epileptic activity induced by restricted bicuculline ejection in the piriform cortex of the isolated guinea pig brain," *J Neurophysiol*, vol. 71, pp. 2463-76, 1994.

[9] L. Librizzi and M. de Curtis, "Epileptiform ictal discharges are prevented by periodic interictal spiking in the olfactory cortex," *Ann Neurol*, vol. 53, pp. 382-9, 2003.

[10] J. J. Chrobak and G. Buzsaki, "Operational dynamics in the hippocampal-entorhinal axis," *Neurosci Biobehav Rev*, vol. 22, pp. 303-10, 1998.

[11] R. J. Staba, C. L. Wilson, A. Bragin, I. Fried, and J. Engel, Jr., "Quantitative analysis of high-frequency oscillations (80-500 Hz) recorded in human epileptic hippocampus and entorhinal cortex," *J Neurophysiol*, vol. 88, pp. 1743-52, 2002.

[12] White, *PNAS*, vol. 97, pp. 8128-8133, 2000.

[13] A. Bragin, C. L. Wilson, J. Almajano, I. Mody, and J. Engel, Jr., "High-frequency oscillations after status epilepticus: epileptogenesis and seizure genesis," *Epilepsia*, vol. 45, pp. 1017-23, 2004.

[14] I. Cohen, V. Navarro, S. Clemenceau, M. Baulac, and R. Miles, "On the origin of interictal activity in human temporal lobe epilepsy in vitro," *Science*, vol. 298, pp. 1418-21, 2002.

[15] R. D. Traub, M. A. Whittington, E. H. Buhl, J. G. Jefferys, and H. J. Faulkner, "On the mechanism of the gamma --> beta frequency shift in neuronal oscillations induced in rat hippocampal slices by tetanic stimulation," *J Neurosci*, vol. 19, pp. 1088-105, 1999.

[16] F. Wendling, F. Bartolomei, J. J. Bellanger, and P. Chauvel, "Epileptic fast activity can be explained by a model of impaired GABAergic dendritic inhibition," *Eur J Neurosci*, vol. 15, pp. 1499-508, 2002.

[17] M. O. Cunningham, C. H. Davies, E. H. Buhl, N. Kopell, and M. A. Whittington, "Gamma oscillations induced by kainate receptor activation in the entorhinal cortex in vitro," *J Neurosci*, vol. 23, pp. 9761-9, 2003.

[18] M. O. Cunningham, D. M. Halliday, C. H. Davies, R. D. Traub, E. H. Buhl, and M. A. Whittington, "Coexistence of gamma and high-frequency oscillations in rat medial entorhinal cortex in vitro," *J Physiol*, vol. 559, pp. 347-53, 2004.
[19] C. J. Wilson HR, "A mathematical theory of the functional dynamics of cortical and thalamic nervous tissue," *Kybernetik*, vol. 13, pp. 55-80, 1973.
[20] W. J. Freeman, "Models of the dynamics of neural populations," *Electroencephalogr Clin Neurophysiol Suppl*, pp. 9-18, 1978.
[21] F. H. Lopes da Silva, A. van Rotterdam, P. Barts, E. van Heusden, and W. Burr, "Models of neuronal populations: the basic mechanisms of rhythmicity," *Prog Brain Res*, vol. 45, pp. 281-308, 1976.
[22] F. H. Lopes da Silva, A. Hoeks, H. Smits, and L. H. Zetterberg, "Model of brain rhythmic activity. The alpha-rhythm of the thalamus," *Kybernetik*, vol. 15, pp. 27-37, 1974.
[23] Z. G. Jansen BH, Brandt ME., "A neurophysiologically-based mathematical model of flash visual evoked potentials.," *Biol Cybern.*, vol. 68, pp. 275-283, 1993.
[24] R. V. Jansen BH, "Electroencephalogram and visual evoked potential generation in a mathematical model of coupled cortical columns.," *Biol Cybern.*, vol. 73, pp. 357-366, 1995.
[25] F. Wendling, J. J. Bellanger, F. Bartolomei, and P. Chauvel, "Relevance of nonlinear lumped-parameter models in the analysis of depth-EEG epileptic signals," *Biol Cybern*, vol. 83, pp. 367-78, 2000.
[26] P. Suffczynski, S. Kalitzin, and F. H. Lopes Da Silva, "Dynamics of non-convulsive epileptic phenomena modeled by a bistable neuronal network," *Neuroscience*, vol. 126, pp. 467-84, 2004.
[27] F. Lopes da Silva, "Electrical potentials," in *Encyclopedia of the human brain*, vol. 2, V. S. Ramachandran, Ed. New York, 2002, pp. 147-167.
[28] M. Muhlethaler, M. de Curtis, K. Walton, and R. Llinas, "The isolated and perfused brain of the guinea-pig in vitro," *Eur J Neurosci*, vol. 5, pp. 915-26, 1993.
[29] M. de Curtis, D. Pare, and R. R. Llinas, "The electrophysiology of the olfactory-hippocampal circuit in the isolated and perfused adult mammalian brain in vitro," *Hippocampus*, vol. 1, pp. 341-54, 1991.
[30] M. de Curtis, A. Manfridi, and G. Biella, "Activity-dependent pH shifts and periodic recurrence of spontaneous interictal spikes in a model of focal epileptogenesis," *J Neurosci*, vol. 18, pp. 7543-51, 1998.
[31] G. Biella and M. de Curtis, "Olfactory inputs activate the medial entorhinal cortex via the hippocampus," *J Neurophysiol*, vol. 83, pp. 1924-31, 2000.
[32] V. Gnatkovsky, L. Uva, and M. de Curtis, "Topographic distribution of direct and hippocampus- mediated entorhinal cortex activity evoked by olfactory tract stimulation," *Eur J Neurosci*, vol. 20, pp. 1897-905, 2004.
[33] L. Uva and M. de Curtis, "Polysynaptic olfactory pathway to the ipsi- and contralateral entorhinal cortex mediated via the hippocampus," *Neuroscience*, vol. 130, pp. 249-58, 2005.
[34] P. D. Bamidis, E. Hellstrand, H. Lidholm, K. Abraham-Fuchs, and A. A. Ioannides, "MFT in complex partial epilepsy: spatio-temporal estimates of interictal activity," *Neuroreport*, vol. 7, pp. 17-23, 1995.
[35] M. Gavaret, J. M. Badier, P. Marquis, F. Bartolomei, and P. Chauvel, "Electric source imaging in temporal lobe epilepsy," *J Clin Neurophysiol*, vol. 21, pp. 267-82, 2004.
[36] M. Witter and F. G. Wouterlood, *The parahippocampal region: organization and role in cognitive function*. New York: Oxford University Press, 2002.

HAL author manuscript inserm-00183634, version 1

HAL author manuscript inserm-00183634, version 1

[37] R. Insausti, M. T. Herrero, and M. P. Witter, "Entorhinal cortex of the rat: cytoarchitectonic subdivisions and the origin and distribution of cortical efferents," *Hippocampus*, vol. 7, pp. 146-83, 1997.

[38] C. L. Dolorfo and D. G. Amaral, "Entorhinal cortex of the rat: topographic organization of the cells of origin of the perforant path projection to the dentate gyrus," *J Comp Neurol*, vol. 398, pp. 25-48, 1998.

[39] C. L. Dolorfo and D. G. Amaral, "Entorhinal cortex of the rat: organization of intrinsic connections," *J Comp Neurol*, vol. 398, pp. 49-82, 1998.

[40] M. Mikkonen, H. Soininen, and A. Pitkanen, "Distribution of parvalbumin-, calretinin-, and calbindin-D28k-immunoreactive neurons and fibers in the human entorhinal cortex," *J Comp Neurol*, vol. 388, pp. 64-88, 1997.

[41] B. N. Hamam, D. G. Amaral, and A. A. Alonso, "Morphological and electrophysiological characteristics of layer V neurons of the rat lateral entorhinal cortex," *J Comp Neurol*, vol. 451, pp. 45-61, 2002.

[42] B. N. Hamam, T. E. Kennedy, A. Alonso, and D. G. Amaral, "Morphological and electrophysiological characteristics of layer V neurons of the rat medial entorhinal cortex," *J Comp Neurol*, vol. 418, pp. 457-72, 2000.

[43] F. G. Wouterlood, M. Vinkenoog, and M. van den Oever, "Tracing tools to resolve neural circuits," *Network*, vol. 13, pp. 327-42, 2002.

[44] T. Gloveli, D. Schmitz, R. M. Empson, T. Dugladze, and U. Heinemann, "Morphological and electrophysiological characterization of layer III cells of the medial entorhinal cortex of the rat," *Neuroscience*, vol. 77, pp. 629-48, 1997.

[45] T. Gloveli, T. Dugladze, D. Schmitz, and U. Heinemann, "Properties of entorhinal cortex deep layer neurons projecting to the rat dentate gyrus," *Eur J Neurosci*, vol. 13, pp. 413-20, 2001.

[46] T. van Haeften, L. Baks-te-Bulte, P. H. Goede, F. G. Wouterlood, and M. P. Witter, "Morphological and numerical analysis of synaptic interactions between neurons in deep and superficial layers of the entorhinal cortex of the rat," *Hippocampus*, vol. 13, pp. 943-52, 2003.

[47] F. G. Wouterlood and H. Pothuizen, "Sparse colocalization of somatostatin- and GABA-immunoreactivity in the entorhinal cortex of the rat," *Hippocampus*, vol. 10, pp. 77-86, 2000.

[48] F. G. Wouterlood, J. C. van Denderen, T. van Haeften, and M. P. Witter, "Calretinin in the entorhinal cortex of the rat: distribution, morphology, ultrastructure of neurons, and co-localization with gamma-aminobutyric acid and parvalbumin," *J Comp Neurol*, vol. 425, pp. 177-92, 2000.

[49] A. Kirchner, J. Breustedt, B. Rosche, U. F. Heinemann, and V. Schmieden, "Effects of taurine and glycine on epileptiform activity induced by removal of Mg2+ in combined rat entorhinal cortex-hippocampal slices," *Epilepsia*, vol. 44, pp. 1145-52, 2003.

[50] J. Breustedt, D. Schmitz, U. Heinemann, and V. Schmieden, "Characterization of the inhibitory glycine receptor on entorhinal cortex neurons," *Eur J Neurosci*, vol. 19, pp. 1987-91, 2004.

[51] M. Funahashi and M. Stewart, "GABA receptor-mediated post-synaptic potentials in the retrohippocampal cortices: regional, laminar and cellular comparisons," *Brain Res*, vol. 787, pp. 19-33, 1998.

[52] N. B. Fountain, J. Bear, E. H. Bertram, 3rd, and E. W. Lothman, "Responses of deep entorhinal cortex are epileptiform in an electrogenic rat model of chronic temporal lobe epilepsy," *J Neurophysiol*, vol. 80, pp. 230-40, 1998.

[53] G. L. Woodhall, S. J. Bailey, S. E. Thompson, D. I. Evans, and R. S. Jones, "Fundamental differences in spontaneous synaptic inhibition between deep and superficial layers of the rat entorhinal cortex," *Hippocampus*, 2004.
[54] F. G. Wouterlood, W. Hartig, G. Bruckner, and M. P. Witter, "Parvalbumin-immunoreactive neurons in the entorhinal cortex of the rat: localization, morphology, connectivity and ultrastructure," *J Neurocytol*, vol. 24, pp. 135-53, 1995.
[55] M. I. Banks and R. A. Pearce, "Kinetic differences between synaptic and extrasynaptic GABA(A) receptors in CA1 pyramidal cells," *J Neurosci*, vol. 20, pp. 937-48, 2000.
[56] M. I. Banks, J. A. White, and R. A. Pearce, "Interactions between distinct GABA(A) circuits in hippocampus," *Neuron*, vol. 25, pp. 449-57, 2000.
[57] R. S. Jones and E. H. Buhl, "Basket-like interneurones in layer II of the entorhinal cortex exhibit a powerful NMDA-mediated synaptic excitation," *Neurosci Lett*, vol. 149, pp. 35-9, 1993.
[58] M. Caballero-Bleda and M. P. Witter, "Projections from the presubiculum and the parasubiculum to morphologically characterized entorhinal-hippocampal projection neurons in the rat," *Exp Brain Res*, vol. 101, pp. 93-108, 1994.
[59] N. Tamamaki and Y. Nojyo, "Preservation of topography in the connections between the subiculum, field CA1, and the entorhinal cortex in rats," *J Comp Neurol*, vol. 353, pp. 379-90, 1995.
[60] T. van Haeften, F. G. Wouterlood, B. Jorritsma-Byham, and M. P. Witter, "GABAergic presubicular projections to the medial entorhinal cortex of the rat," *J Neurosci*, vol. 17, pp. 862-74, 1997.
[61] F. G. Wouterlood, T. Van Haeften, M. Eijkhoudt, L. Baks-Te-Bulte, P. H. Goede, and M. P. Witter, "Input from the presubiculum to dendrites of layer-V neurons of the medial entorhinal cortex of the rat," *Brain Res*, vol. 1013, pp. 1-12, 2004.
[62] S. Craig and S. Commins, "Interaction between paired-pulse facilitation and long-term potentiation in the projection from hippocampal area CA1 to the entorhinal cortex," *Neurosci Res*, vol. 53, pp. 140-6, 2005.
[63] M. Pikkarainen, S. Ronkko, V. Savander, R. Insausti, and A. Pitkanen, "Projections from the lateral, basal, and accessory basal nuclei of the amygdala to the hippocampal formation in rat," *J Comp Neurol*, vol. 403, pp. 229-60, 1999.
[64] M. P. Witter, G. W. Van Hoesen, and D. G. Amaral, "Topographical organization of the entorhinal projection to the dentate gyrus of the monkey," *J Neurosci*, vol. 9, pp. 216-28, 1989.
[65] J. M. Wyss, "An autoradiographic study of the efferent connections of the entorhinal cortex in the rat," *J Comp Neurol*, vol. 199, pp. 495-512, 1981.
[66] M. P. Witter, H. J. Groenewegen, F. H. Lopes da Silva, and A. H. Lohman, "Functional organization of the extrinsic and intrinsic circuitry of the parahippocampal region," *Prog Neurobiol*, vol. 33, pp. 161-253, 1989.

HAL author manuscript inserm-00183634, version 1

HAL author manuscript inserm-00183634, version 1

Legends:

Table1: Table of input subpopulation indexes as used for equations writing. Each source subpopulation (P1, P2: pyramidal cells. St: stellate cells. Exc: excitatory. Inh: inhibitory. IN: interneurons) has been conventionally numbered from 1 to 12 and the different types of neurotransmission (I: inhibitory and E: excitatory) are denoted in the first colon, line 3 to line 7 with the corresponding neurotransmitter in brackets. The connectivity oriented graph represented on figure 1-A is encoded in the table cells: an empty cell for no afference, else the list of existing afferences. The last line indicates noise input applied to P_1, P_2 and St subpopulations.

Table 2: Amplitude of average post-synaptic potentials (initial values for which normal background activity is simulated) and time constants used in the model

Table 3: Local connectivity constants in EC model

Figure 1: (A) Cellular organization (P1, P2: pyramidal cells. St: stellate cells. Exc: excitatory. Inh: inhibitory. IN: interneurons) of the EC established from literature review about cytoarchitectonic and neurobiological data. This was used as the starting point in the EC model design. From generic input/output diagram (B) representing all inputs and the output for any neuronal population and mathematical conversions (transfer functions, sigmoid function), a particularized diagram for the pyramidal subpopulation in deep layers (P2) is given as example (C).

Figure 2: The different types of activity produced by the model and comparison with real field potentials recorded from EC in isolated guinea-pig brain. In figure 4, each type of activity is coded by the color indicated in corresponding box.

Figure 3: For each type of activity, spectral (frequency bands: 3-12 Hz; 13-17 Hz; 18-30 Hz) and statistical (number of points in interval -60/-5 %; -5/5 %; 5/60 %) features included in the features vector used to perform the classification are represented.

Figure 4: Activity maps obtained for model exploration with respect to I_1 ($GABA_{a\ slow}$ receptor-mediated inhibition) and I_2 ($GABA_{a\ fast}$ receptor-mediated inhibition) parameters corresponding to the synaptic gains in feedback loops from inhibitory interneurons to pyramidal cells in deep layers of EC. Limit values (illustrated by a solid line) in the two-dimensional parameters plane I_1/I_2 separating the stable from the unstable parameter regions in the model (based on stability study) is superimposed on each activity map. Stable (respectively unstable) region appears on the right (respectively left) side of the line. For two maps (I_3=6.5 and I_3=8), closed contours were observed inside which stability was found.

Figure 5: (A) Typical seizure pattern recorded from EC in the isolated guinea-pig brain perfused with bicuculline. Eight phases can be distinguished in this pattern (see details in text). (B) Corresponding simulated signals generated by the model for each phases from synaptic gains profiles defined by the path drawn on activity maps. (C) One possible path on activity maps explaining the transitions of activity observed in the real field potential recording (A).

HAL author manuscript inserm-00183634, version 1

Figure 6: (A) another seizure pattern characterized by the lack of rhythmic spikes and fast activity at the seizure onset. In this pattern, six phases can be distinguished (see details in text). (B) Corresponding simulated signals produced in the model for each phases from synaptic gains profiles defined by the path drawn on activity maps (see (C)). One possible path on activity maps (C) explaining the transitions of epileptic activity observed in the real field potential recording (A) assuming that $GABA_{a\ slow}$ receptor-mediated inhibition decreases less abruptly and in a lesser extent. Another possible path on one activity map (D) explaining the transitions observed from background activity to the seizure activities in real recordings (A) with hypothesis that $GABA_b$ receptor-mediated inhibition is strong.

HAL author manuscript inserm-00183634, version 1

HAL author manuscript inserm-00183634, version 1

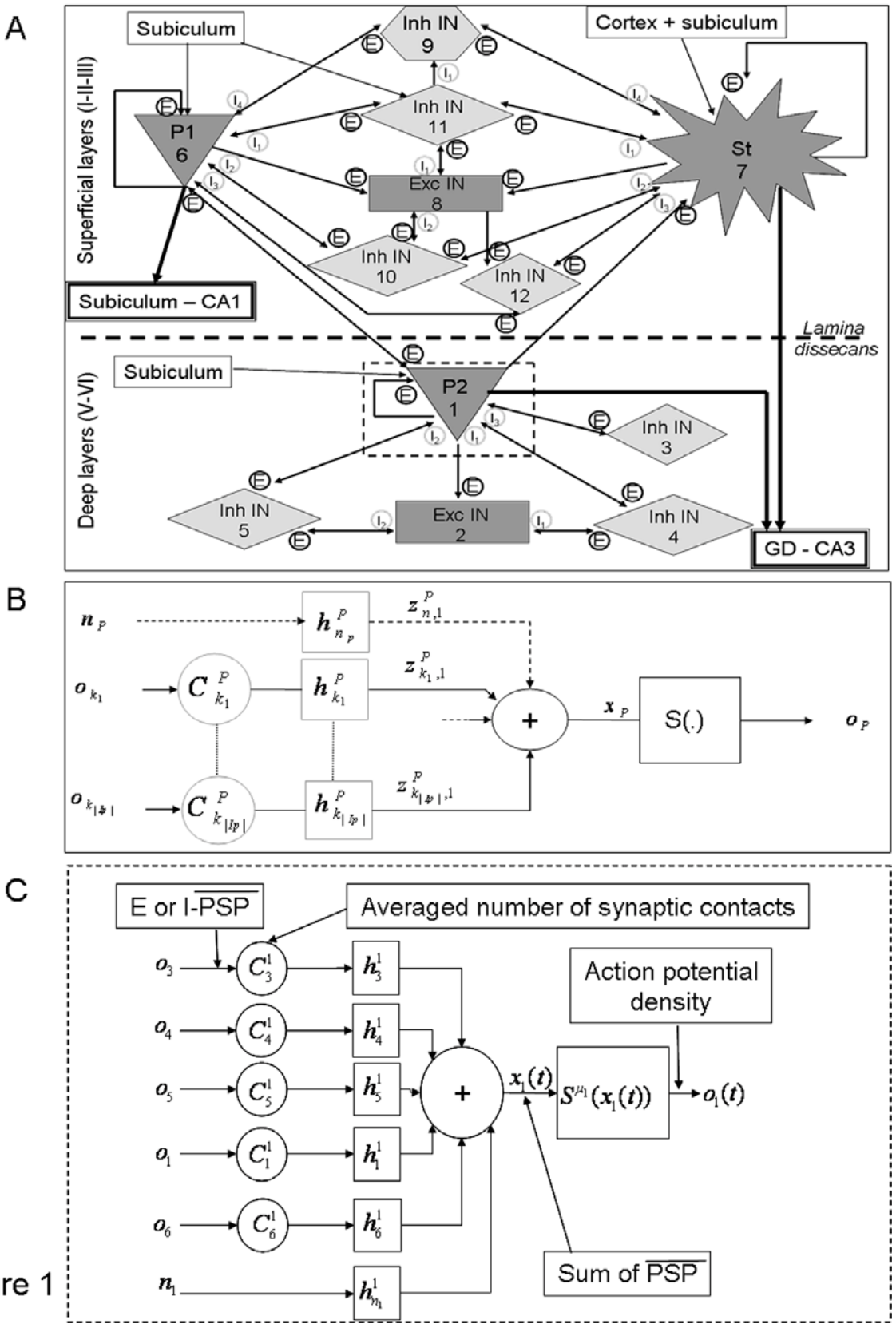

Figure 1

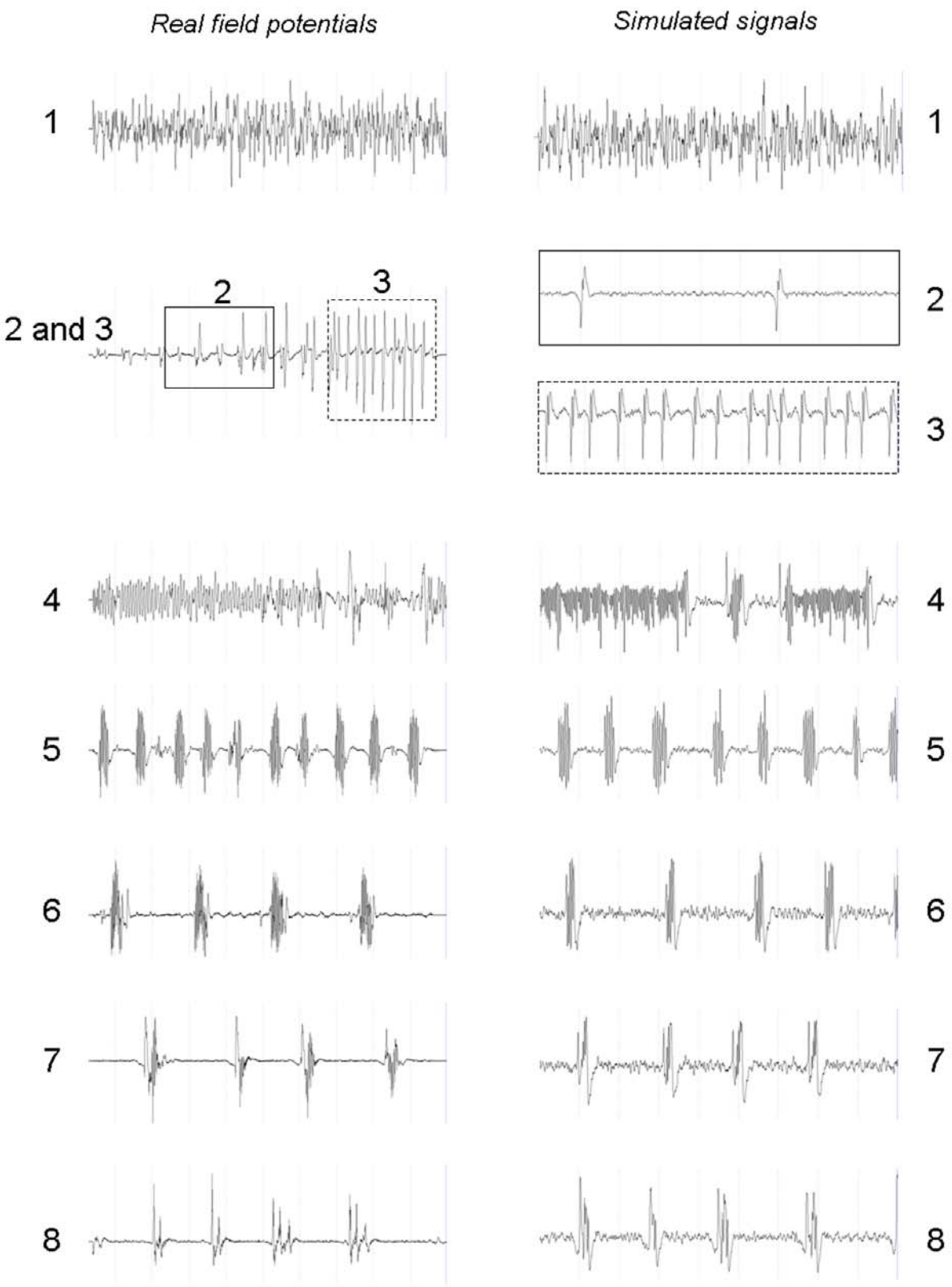

Figure 2

HAL author manuscript inserm-00183634, version 1

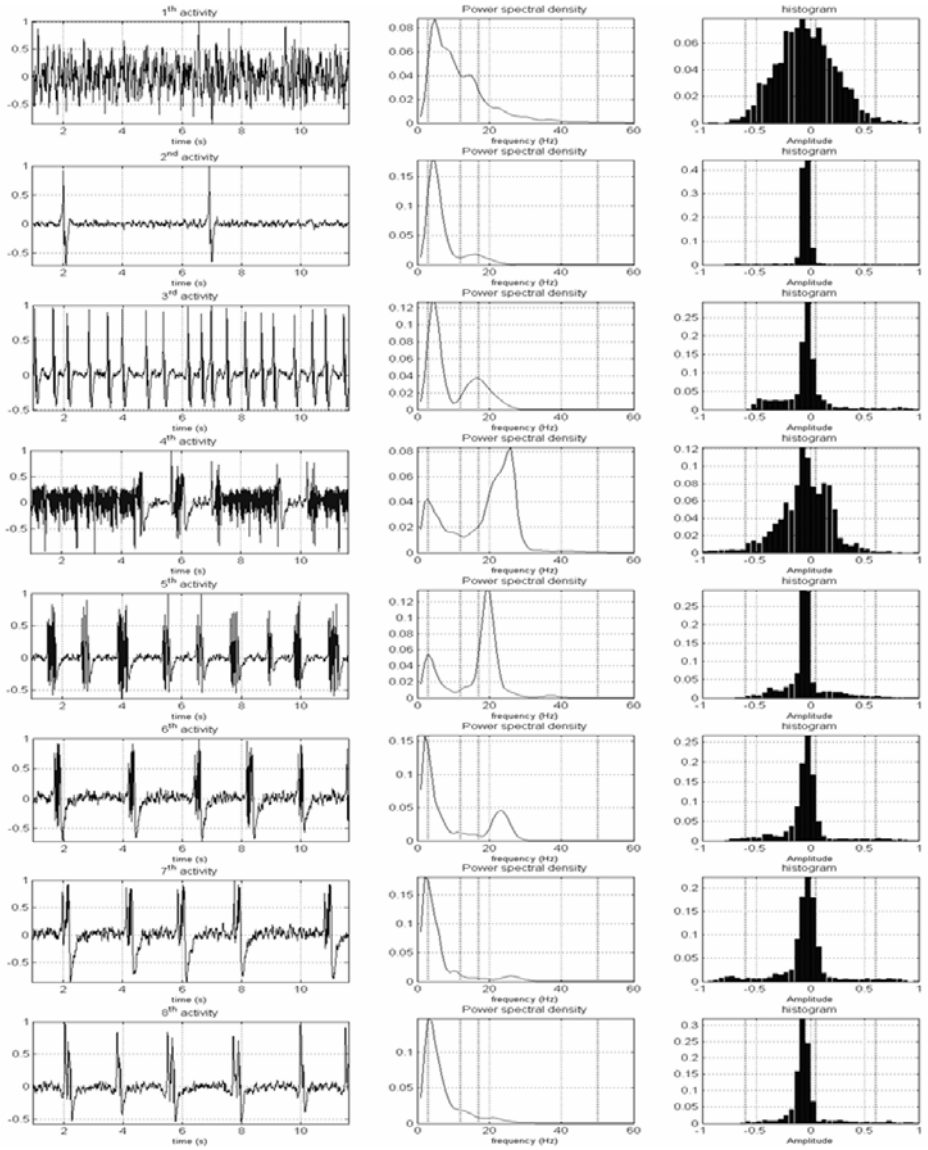

Figure 3

HAL author manuscript inserm-00183634, version 1

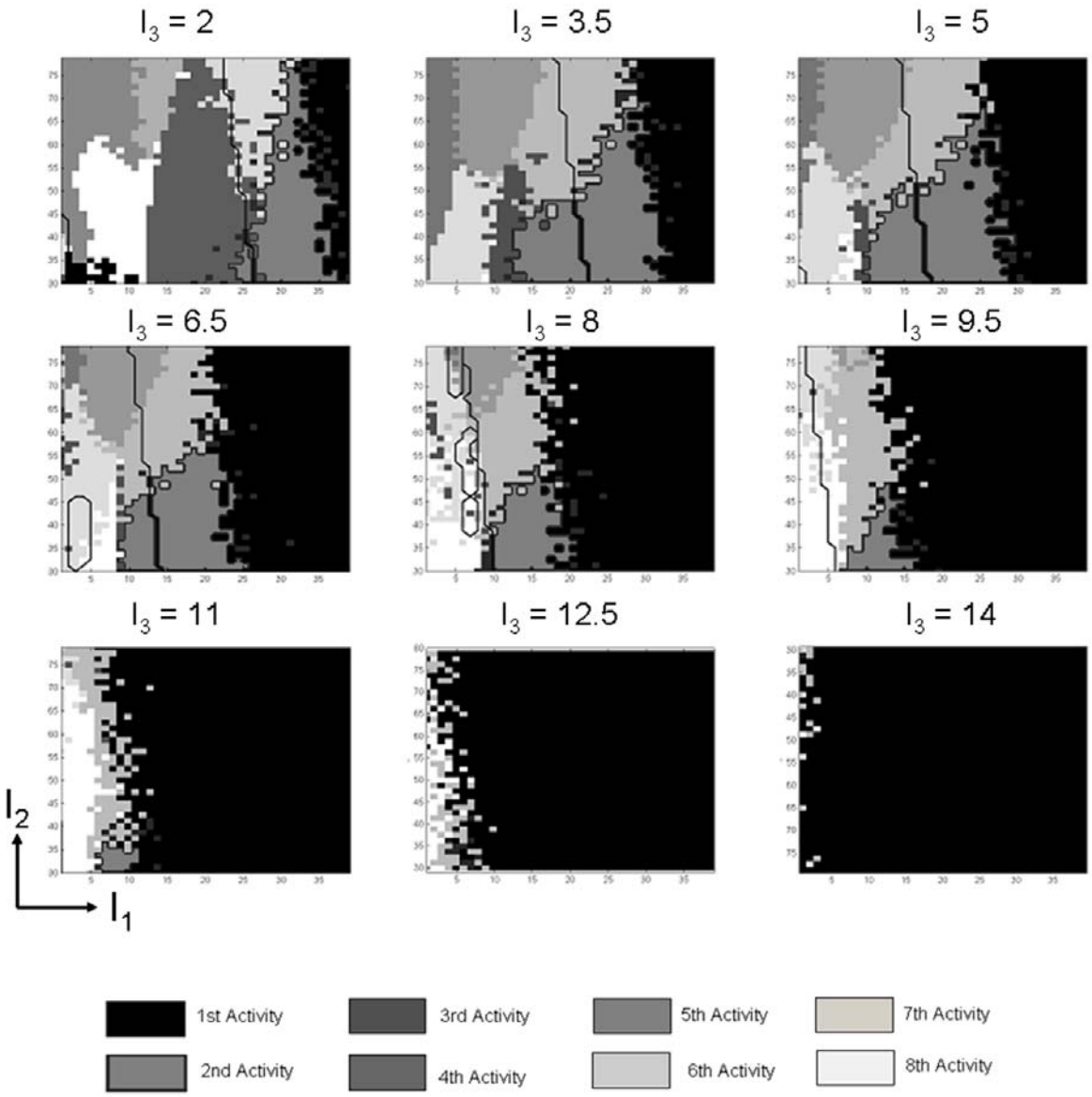

Figure 4

HAL author manuscript inserm-00183634, version 1

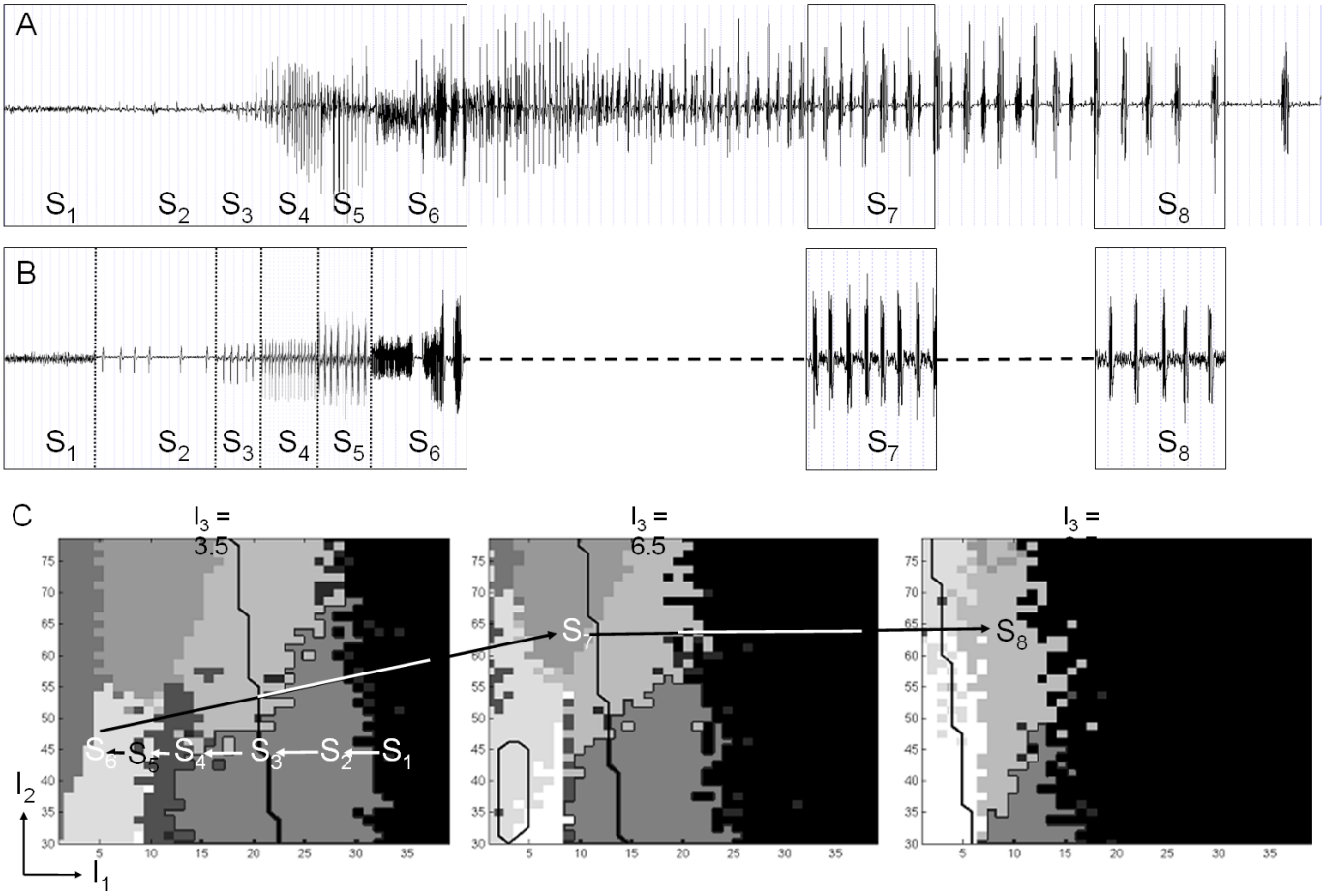

Figure 5

HAL author manuscript inserm-00183634, version 1

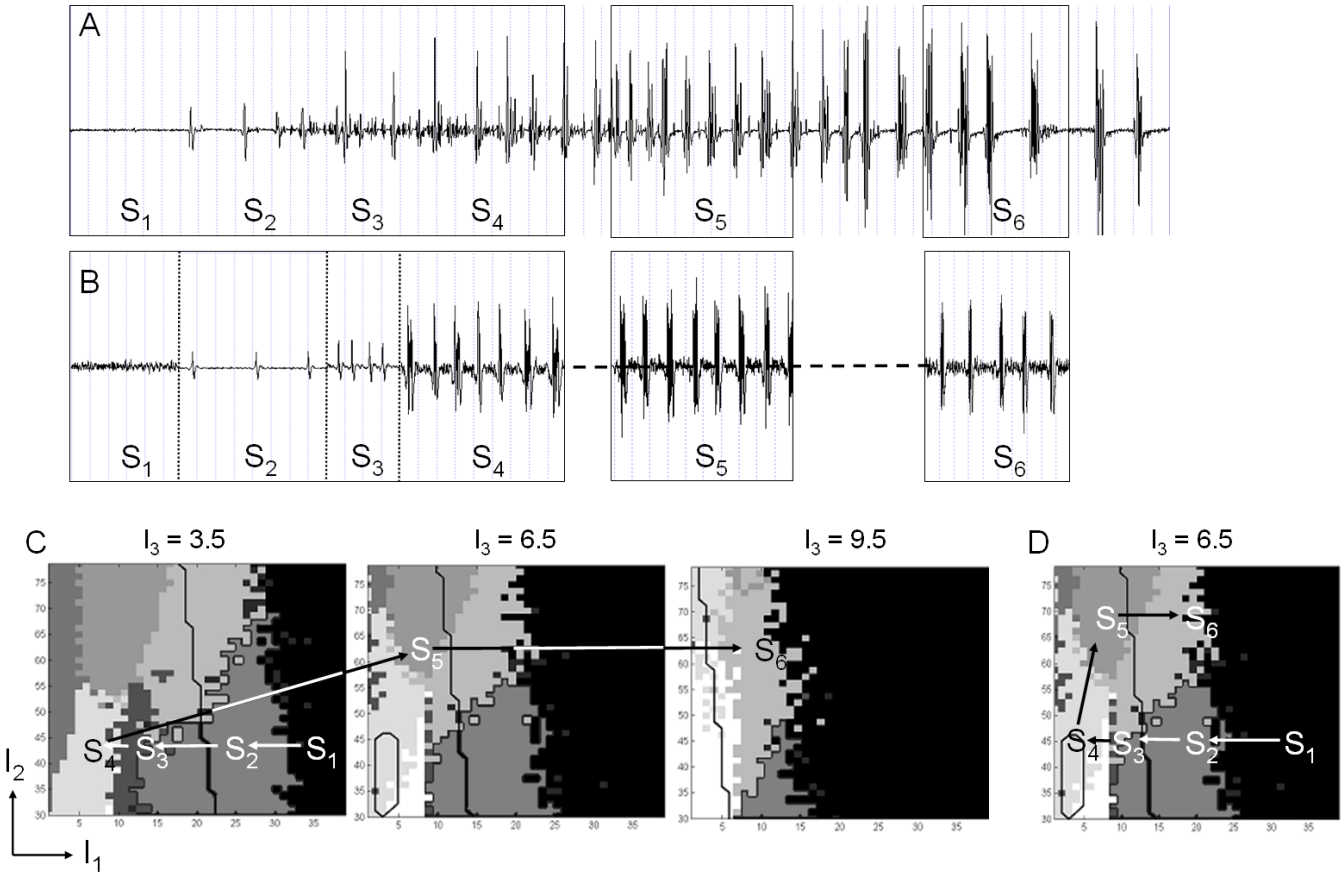

Figure 6

HAL author manuscript inserm-00183634, version 1

Table 1:

Layers	DEEP					SUPERFICIAL						
Neuronal population type / Neurotransmission type	1	2	3	4	5	6	7	8	9	10	11	12
	P2	Exc IN	Inh IN	Inh IN	Inh IN	P1	St	Exc IN	Inh IN	Inh IN	Inh IN	Inh IN
I1 ($GABA_{a, slow}$)	4	4				11	11	11	11			
I2 ($GABA_{a, fast}$)	5	5				10	10	10				
I3 ($GABA_b$)	3					12	12					
I4 (Glycine)						9	9					
E (Glutamate)	1, 6	1	1	1, 2	1, 2	1, 6	1, 7	6,7	6,7	6, 7, 8	6, 7, 8	6,7, 8
N	n2					n1	n3					

HAL author manuscript inserm-00183634, version 1

Table 2:

	DEEP	SUPERFICIAL	
	Average amplitude (mV)	Average amplitude (mV)	Time constants (ms)
Excitatory PSP (Glutamate)	$E = 6$	$E = 3$	$\tau_e = 10$
Inhibitory PSP ($GABA_{a,\ slow}$)	$I_1 = 25$	$I_1 = 25$	$\tau_1 = 30$
Inhibitory PSP ($GABA_{a,\ fast}$)	$I_2 = 40$	$I_2 = 40$	$\tau_2 = 4$
Inhibitory PSP ($GABA_b$)	$I_3 = 5$	$I_3 = 5$	$\tau_3 = 300$
Inhibitory PSP (Glycine)	Not present	$I_4 = 40$	$\tau_4 = 27$

HAL author manuscript inserm-00183634, version 1

Table 3:

k \ p	P_1	P_2	St	IN exc	IN $_{GABAa,s}$	IN $_{GABAa,f}$	IN $_{GABAb}$	IN $_{Gly}$
P_1	160	4	4	50	50	50	50	30
P_2	3	160	-	50	50	50	50	-
St	-	-	160	50	50	50	50	50
IN exc	-	-	-	-	20	20	20	-
IN $_{GABAa,s}$	35	35	35	20	-	-	-	10
IN $_{GABAa,f}$	25	25	25	20	-	-	-	-
IN $_{GABAb}$	15	15	15	-	-	-	-	-
IN $_{Gly}$	-	35	35	-	-	-	-	-

HAL author manuscript inserm-00183634, version 1